Predicting the leaf water potential of potato plants using RGB reflectance

R. Zakaluk[1] and R. Sri Ranjan[2]*

*[1]Civil Engineering Technology Department, Red River College, Winnipeg, Manitoba R3H 0J9, Canada; and [2]Department of Biosystems Engineering, University of Manitoba, Winnipeg, Manitoba R3T 5V6, Canada. *Email: ranjan@cc.umanitoba.ca*

Zakaluk, R. and Sri Ranjan, R. 2008. **Predicting the leaf water potential of potato plants using RGB reflectance**. Canadian Biosystems Engineering/Le génie des biosystèmes au Canada **50**: 7.1-7.12. Existing plant water status measurements are impractical to meet real time irrigation monitoring requirements. This research explored the use of artificial neural network (ANN) modeling of images captured by a ground-based, five megapixel, RGB (red green blue) digital camera to predict the leaf water potential (Ψ_L) of field grown potato plants. Leaf water potential, soil nitrate (N) content, and volumetric water content were obtained along with digital images in randomly selected sample plots. The images from all the plots were radiometrically calibrated and then classified to isolate green foliage from soils, flowers, shadows, and senescent leaves. The RGB images, six image transformations, and nine vegetation indices were transformed using principal components analysis (PCA). Findings showed a significant inverse linear relationship between soil N and leaf reflectance in the G image band (r = -0.71, p = 0.003) and that the ANN model input neuron weights with more separation between soil N and Ψ_L were most important in predicting Ψ_L. For the ANN model validation dataset, findings indicated that the measured and predicted Ψ_L distributions were normally distributed (W_{meas} = 0.97, p = 0.8, W_{pred} = 0.95, p = 0.6), the means were not significantly different (t = -1.00, p =0.3), and the variances were equal (F = 0.14, p = 0.7). Based on these results, the ground-based digital camera proved to be an adequate sensor for image acquisition and a practical tool for predicting Ψ_L of potato plants. **Keywords:** nitrate, IHS transformation, chromaticity transformation, principal components, vegetation indices, remote sensing, artificial neural network, digital camera.

Les méthodes courantes de mesure de teneur en eau des plantes sont inappropriées pour la gestion en temps réel des systèmes d'irrigation. Cette étude a exploré l'utilisation de la modélisation par un réseau neuronal artificiel d'images prises par une caméra digitale fixe RGB (rouge vert bleu) de cinq mégapixels pour prédire le potentiel hydrique des feuilles (Ψ_L) d'un champ de plants de pommes de terre. Le potentiel hydrique des feuilles, la teneur en nitrate (N) et la teneur en eau du sol sur une base volumique ont été mesurés et des photographies digitales ont été prises dans des parcelles sélectionnées de manière aléatoires. Les images de toutes les parcelles étaient calibrées sur le plan radiométrique pour ensuite être classifiées dans le but d'isoler le feuillage vert du sol, des fleurs, des ombres et des feuilles sénescentes. Les images RGB, six transformations d'images et neuf indices de végétation ont été transformés en utilisant l'analyse des composantes principales (ACP). Les résultats ont démontré une relation linéaire inverse entre la teneur en N du sol et la réflexivité des feuilles dans la bande d'image G (r = -0,71, p = 0,003). Une pondération plus importante entre la teneur en N du sol et Ψ_{et} au niveau du modèle neuronal d'intrant 'ANN' était plus importante pour la prédiction de Ψ_L. Pour les données obtenues avec le modèle ANN validé, les résultats ont indiqué que la distribution des valeurs mesurées et prédites de Ψ_L avaient une distribution normale (W_{mesur} = 0,97, p = 0,8, $W_{préd}$ = 0,95, p = 0,6) ; les moyennes n'étaient pas différentes (t = -1,00, p =0,3) et les variances étaient égales (F = 0,14, p = 0,7). Considérant ces résultats, une caméra digitale fixe s'est avérée être un senseur adéquat pour l'acquisition d'images et un outil pratique pour prédire Ψ_L des plants de pommes de terre. **Mots clés**: nitrate, transformation IHS, transformation chromatique, composantes principales, indices de végétation, senseur à distance, réseau neuronal artificiel, caméra digitale.

INTRODUCTION

Water is essential for plant growth and sustenance. According to Bowman (1989), a decrease in plant water content causes a decrease in stomatal conductivity that limits the uptake of carbon dioxide for photosynthesis. Problems for potato (*Solanum tuberosum* L.) producers are created because plant water stress on potato inhibits photosynthesis and causes a decrease in total biomass and a decrease in both fresh and dry matter tuber yield (Costa et al. 1997; Gunel and Karadogan 1998). The leaf water potential (Ψ_L), a measure of the negative pressure that exists within the leaf cells, can be used to measure plant water status. The negative pressure results from stomatal resistance which causes water to flow from the roots toward the leaf. The dynamic nature of plant water status over a given 24-h period (Scholander et al. 1965; Waring and Cleary 1967), however, makes in situ plant water status measurement impractical for irrigation scheduling over large areas.

Remote sensing either by airborne or spaceborne image acquisition methods is a tool with the potential to monitor plant water status over large areas (Bastiaanssen and Bos 1999; Jackson et al. 2004; Karimi et al. 2005). Previous research advocates the use of the short wave infrared (SWIR) region to model plant water content (Ceccato et al. 2002a, 2002b; Ripple 1986). However, the addition of an imaging sensor in the SWIR water absorption regions for vegetation at 1450, 1950, and 2600 nm (Ustin 2004) to an irrigation scheduling system would be cost prohibitive. Imaging sensors that model plant water status in the visible region would therefore be more economically viable for an irrigation scheduling system. Justification for using visible light reflectance as an indicator of plant water status is based on the interrelationships between plant water status, photosynthesis, and irradiance load on the leaf (Carter 1991; Schlemmer et al. 2005; Wheeler 2006). Zakaluk and Sri Ranjan (2007) found that an RGB (red green blue) digital camera could determine Ψ_L under greenhouse conditions. The objective of this study was to explore the use of a digital camera to acquire images, in the visible region, of a field grown potato crop under different plant water levels and different soil nitrate conditions.

Fig. 1. Study area location (approximately 130 km south-west of Winnipeg, Manitoba).

Changes in nitrogen and water availability result in physiological changes in the plant that alter leaf reflectance in the visible region (Penuelas et al. 1994; Schlemmer et al. 2005; Zhurmar and Yanovskaya 1992). Specifically, soil or plant nitrogen levels are associated with plant greenness (Blackmer et al. 1994; Boegh et al. 2002; Osborne et al. 2002; Schlemmer et al. 2005; Thomas and Oerther 1972). In addition, plant nitrogen levels are associated with chlorophyll content (Haboudane et al. 2002; Schlemmer et al. 2005). Plant nitrogen levels are also related to the light energy incident upon the leaf surface and photosynthesis (Charles-Edwards et al. 1986). Since soil and plant nitrogen interacts with chlorophyll content, photosynthesis, and reflectance in the visible spectral region research, exploring leaf reflectance in the visible region to determine Ψ_L must consider nitrate (N) levels in either the soil or plant.

To solve the problem of measuring plant water status for irrigation using remote sensing, an economical sensor with rapid image delivery and flexible revisit rates must be employed. Commercially available digital cameras are one possible solution to meeting the requirements of applying remote sensing for measuring plant water status using leaf reflectance in the visible region. In this study, therefore, using a camera equipped with a single five megapixel full frame sensor, RGB digital images were explored to determine the Ψ_L of field grown potato (*Solanum tuberosum* L. var. cv. Sangre) using artificial neural network (ANN) modelling under different soil N levels. The following questions were addressed:

1. Can 0.91 mm spatial resolution RGB images separate foliage from shadow, soils, leaf senescence, and flowers?
2. Is there a relationship between soil N and leaf reflectance in the green image band?
3. Can ANN modelling of RGB images determine Ψ_L of potatoes (*Solanum tuberosum* L. var. cv. Sangre) under field conditions?
4. Are there relationships between Ψ_L and soil N that influence the relative importance of the input neurons in the ANN model?
5. Can a ground-based digital camera supply RGB images as an alternative to airborne-spaceborne imaging sensors?

METHODS

Agronomic instruments and measurements

A pressure chamber instrument (PMS Model 600, PMS Instrument Company, Albany, OR) was used to collect leaf water potential, Ψ_L (MPa). Soil N (0-150 mm) was determined using a hand-held Nitrachek™ 404 Reflectometer (KPG Products Ltd., Hove, East Sussex, UK) and Merkoquant® N test strip (Merck KGaA, Darmstadt, Germany) using the method described by Tremblay et al. (2001).

Imaging sensor and platform

A five megapixel, single, charged couple device (CCD) chip, Sony DSC-T1 digital full frame camera using a 35-mm camera equivalent focal length of 38 mm, capturing 2592 x 1944 pixel images, was used to acquire images. The size of each detector on the CCD chip was 2.775 x 2.775 µm. The peak wavelengths were empirically determined to be 610, 520, and 460 nm for the R, G, and B filters, respectively (Sony Corporation 2004). The digital camera was operated by remote control and mounted on a telescopic pole that extended 2.5 m above ground level (AGL) covering 2.37 x 1.78 m on the ground. The ground spatial resolution of each pixel was 0.91 x 0.91 mm.

Experimental design

Data were collected in a 29-ha field (Fig. 1) located approximately 130 km southwest of Winnipeg, Manitoba (49^0 16.198' N, 98^0 3.146' W) during cloud free periods. In the previous fall, nitrogen fertilizer was not applied to the field. The field consisted of coarse-loamy soils with drainage tile and an irrigation pivot. The field was planted with a Sangre, red potato variety (*Solanum tuberosum* L. cv. Sangre). Liquid nitrogen fertilizer (28-0-0) was applied to the field at the rate of 66 kg/ha on the 35^{th} day after planting (DAP).

To avoid disruption for the crop producer, the soil N and Ψ_L factors were sampled using a systematic approach with a random start. Nine plots were identified at both the southwest and southeast corners of the field using a 45 x 45 m grid for a total of 18 plots. To assess the influence of soil N on Ψ_L, soil tests (0–150 mm) were carried out using twelve soil samples per plot to obtain an average soil N level at each plot. Field corners made it logistically possible to collect field data by reducing the travel time between plots and thus maximizing the number of plots that could be sampled in a day. The outcome of a k-means classifier on the undetermined number of soil N levels over 18 sample plots was five. In each plot, three rows of potatoes, each approximately 2 m long, were selected (Fig. 2). Thus each sample plot contained three replicates or rows with three plants sampled from each replicate. During the sampling period, plots were randomly sampled to collect data on Ψ_L measures and images. Images were acquired during cloud free periods, from 10:00 to 16:00 h central standard time across the tuber initiation, tuber bulking, and tuber maturation growth stages. After image acquisition, Ψ_L measurements were taken within 30 minutes. This plot design offered maximum flexibility for later data analysis of Ψ_L and soil N measurements by allowing for the calculation of a whole plot average from all measurements within a plot or a whole row average from all measurements in a row.

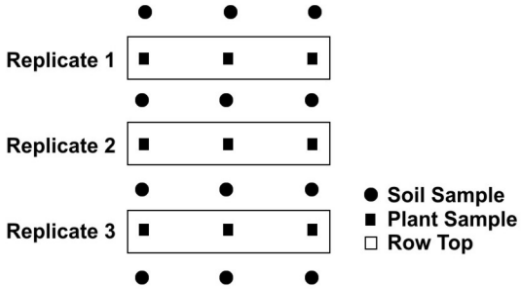

Fig. 2. Layout for sample plots for soil N and Ψ_L.

Image radiometric calibration

Due to differences in illumination resulting from changes in the solar zenith angle within and across periods of image capture, each image was radiometrically calibrated before the images were analyzed. At each sample plot, a 20-step gray scale reflectance standard (Klotz et al. 2003) was imaged at the beginning of the image acquisition process. Since the contrast of each image was unaffected by differences in illumination, the average reflectance value (RV) from the reflectance standard was used to generate radiometric calibration coefficients (Gonzalez and Woods 2002). For each RGB image band, radiometric calibration coefficients were generated for each day of image capture by obtaining the average RV from the reflectance standard imaged at each plot on a given day and standardizing them to the mean RV of the 8-bit image scale. Using an additive model, the radiometric calibration coefficients were then applied to each uncorrected image band for the respective day of acquisition to create radiometrically calibrated RGB images across the study period. The purpose of radiometric image calibration was to standardize the intensity (I) of RGB RVs for all images across all image acquisition dates.

Foliage classification

The visible region can be used for estimates of green plant coverage (Gitelson et al. 2002; McCoy 2005; Woebbecke at al. 1995). To remove the effects of shadow, soils, leaf senescence, and flowers (background noise) on reflectance values, the foliage was classified to isolate green plants within the canopy architecture. Before the foliage was classified, the radiometrically calibrated images were mosaiced together to create one RGB image of all plots and rows for all dates imaged in the study. An unsupervised approach was then used to classify the mosaiced image for foliage and background noise using the iterative self-organizing data analysis technique (ISODATA) clustering algorithm (del Moral 1975). The unsupervised classification approach involved generation of spectral clusters for all data in spectral space by the ISODATA classifier followed by observation-based labeling of the spectral clusters for green foliage and background noise. Image classification was performed using PCI ImageWorks (Version 9.0) software. Using the RGB image bands for input, a minimum and maximum of 254 spectral classes were specified. To refine the number of class means and class boundaries, a total of 254 iterations was requested with a maximum within-class difference of 10 SD, overall cluster mean movement threshold of 0.01%, minimum cluster splitting threshold of 5 samples, maximum number of class pairs that can be lumped per iteration of 5, and a lumping distance of 1 between classes. The spectral region identified as green foliage was then used as a mask on the mosaic to extract a mean RV for each RGB band and each plot row. Thus all portions of the foliage falling within shadow, soils, leaf senescence, and flowers were eliminated from further analysis. While other techniques could be used to obtain a vegetation mask (Gitelson et al. 2002; White et al. 2000), the use of the unsupervised image classification technique served as a tool to isolate green foliage from background noise without the need for further validation.

Image transformations and band ratios

More spectral information can be obtained from the RGB images through the use of image transformations and band ratios (Asrar et al. 1984), henceforth referred to as vegetation indices (Table 1). Three simple ratio (SR) vegetation indices based on the ratio between two image bands (Table 1, Eqs. 1 – 3) were used in this study. Previous research has used similar simple ratios (Gamon and Surfas 1999; Kanemasu 1974; McMurtrey et al. 1994). In addition to the SR vegetation indices, three normalized difference (ND) vegetation indices (Table 1, Eqs. 4 – 6) were calculated to determine their usefulness for modeling Ψ_L measurements (Gitelson et al. 2002). Vegetation indices focusing on the visible spectrum were calculated using the extracted RV means to explore their utility in modeling Ψ_L measurements.

To obtain additional spectral information, an intensity (I), hue (H), and saturation (S) color coordinate transformation (Table 1, Eqs. 7 – 9) was first calculated (Jensen 2005). An X, Y, Z chromaticity color coordinate transformation (Table 1, Eqs. 10 – 12) was also calculated (Gillespie et al. 1987). Finally, vegetation indices based on slope were defined. Slope derived vegetation indices are the difference in spectral reflectance between two image bands standardized by the difference between the peak wavelengths used by the image bands and can be described as "rise" over "run" equations (Table 1, Eqs. 13 – 15). The use of vegetation indices that might prove beneficial in the determination of Ψ_L measurements was undertaken to provide additional spectral information not found in the RGB bands.

Data analysis

To establish whether Ψ_L could be determined using the digital camera, the RGB and vegetation index results were compared to the respective Ψ_L measurements. To contradict the ability of ANN models to learn from a random set of generated numbers (Rzempoluck 1998), a cross validation approach was used. A random selection of 75% of the dataset was used for ANN training while the remaining 25% of the dataset was used to validate the ANN modeling results.

The training and validation dataset distributions were checked for: normality using the Shapiro-Wilk (W) test, unequal variance using Bartlett's test for unequal variance (F), and differences between means using the student's *t* test (SAS Institute 2002). Where required to fulfill the assumption of normality, either logarithmic (log) or exponential (X) data transformations were applied. Image variables that did not meet the assumption of normality were dropped from further analysis. If a given image variable with a normal distribution indicated significant unequal variance or a significant difference between training and validation dataset means, these too were dropped

Table 1. Vegetation indices derived from the RGB images.

Equation		Nomenclature
$GB = \frac{G}{B}$	(1)	GB = green blue simple ratio G = green image band B = blue image band
$RB = \frac{R}{B}$	(2)	RB = red blue simple ratio R = red image band
$GR = \frac{G}{R}$	(3)	GR = green red simple ratio
$NDGRI = \frac{G-R}{G+R}$	(4)	NDGRI = normalized difference green red index
$NDGBI = \frac{G-B}{G+B}$	(5)	NDGBI = normalized difference green blue index
$NDRBI = \frac{R-B}{R+B}$	(6)	NDRBI = normalized difference red blue index
$I = R+G+B$	(7)	I = intensity
$H = \frac{G-B}{I-3B}$	(8)	H = Hue
$S = \frac{I-3B}{I}$	(9)	S = saturation
$X = \frac{R}{B+G+R}$	(10)	X = red X transformation
$Y = \frac{G}{B+G+R}$	(11)	Y = green Y transformation
$Z = \frac{B}{B+G+R}$	(12)	Z = blue Z transformation
$GBS = \frac{G-B}{GPWL-BPWL}$	(13)	GBS = green blue slope transformation GPWL = peak wavelength (nm) of the green image band BPWL = peak wavelength (nm) of the blue image band
$GRS = \frac{G-R}{GPWL-RPWL}$	(14)	GRS = green red slope transformation RPWL = peak wavelength (nm) of the red image band
$RBS = \frac{R-B}{RPWL-BPWL}$	(15)	RBS = red blue slope transformation

from further analysis. A significance level (α) of 5% was used for all primary statistics. Thus, image parameters for the training and validation datasets with normal distributions, no significant unequal variance, and no significant difference between means were then considered to be candidates for principal component analysis (PCA).

Principal component analysis is a data compression technique that reduces the number of variables into principal component factors that can be more interpretable than the original variables (Eastman and Fulk 1993; Ingebritsen and Lyon 1985). The goal of PCA was to reduce linear dependency among image variables or input neuron candidates while maximizing collinearity with Ψ_L measurements.

The primary statistics used in this study to evaluate results of the ANN model on the measured Ψ_L and predicted Ψ_L for the validation dataset were the W test, F test, *t* test, and coefficient of variance (CV). The W test was used to compare distributions, the *t* test was used to determine if there was no difference between measured Ψ_L and predicted Ψ_L means, while the F test for unequal variance and CV were used as respective indicators of measured Ψ_L and predicted Ψ_L variability, plus experimental error. The goal of the statistical analysis was to determine if both the measured Ψ_L and predicted Ψ_L for the validation dataset were from common populations.

Finally, given that this research was carried out in a production field, the strength of the *t* test was evaluated by calculating the least significant value. Determining the strength of the *t* test provided an indication of how small a difference was detectable between measured Ψ_L and predicted Ψ_L in the validation data.

The contributions of each input neuron for the ANN model were assessed using the relative importance (RI) of respective neuron connection weights (Gevrey et al. 2003). The image loadings of each principal component (PC) used as an input neuron were also examined using Pearson's correlation coefficient (r). Examination of the RI and PC image loadings enables the investigator to rationalize the value of input neurons and clarify the "black-box" nature of the ANN model.

RESULTS

Row averages were chosen as the sample measure due to foliage overlap within rows, ruling out individual plant delineation. Row averaging resulted in a total of 73 rows or samples across all plots and soil N levels over the sampling period. Two rows were missing due to a lack of image coverage. Given that the goal of irrigation is to avoid over-watering the plant or having the plant water status decline to the permanent wilting point, the dataset was limited to the range of well-watered plants. The resulting dataset consisted of 52 samples, split into 39 samples for training the ANN model and 13 samples for validating the ANN model.

Foliage classification

The spectral relationship between the R and G image bands was used to label the 254 spectral classes derived from the ISODATA classification (Fig. 3). All spectral classes were

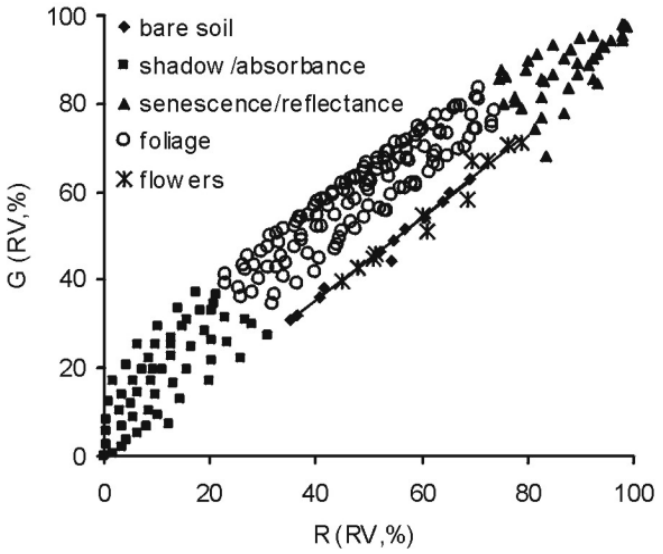

Fig. 3. Spectral relationship between RG bands for foliage classification. Note that the bare soil/flower separation line is perpendicular to green foliage.

labeled for: shadow, soils, leaf senescence, and flowers (background noise), as well as foliage. Definitive decision boundaries in spectral space were identified for all background noise and foliage. Using the R and G image bands, the green leaf pigment decision boundaries within the foliage of the canopy were perpendicular to a soil and flower line; between shadow, soil, and leaf senescence. Although a mosaic of all images may appear as a study limitation, given that each image was radiometrically calibrated before mosaicing and that the number of spectral clusters was maximized during classification, there was no benefit to classifying each image independently. Classification results for all forms of background noise and foliage would appear in the same pattern and the same decision boundaries. On the other hand, an image classification approach may not be viable under less homogeneous vegetation canopies such as natural forest stands which contain more heterogeneous

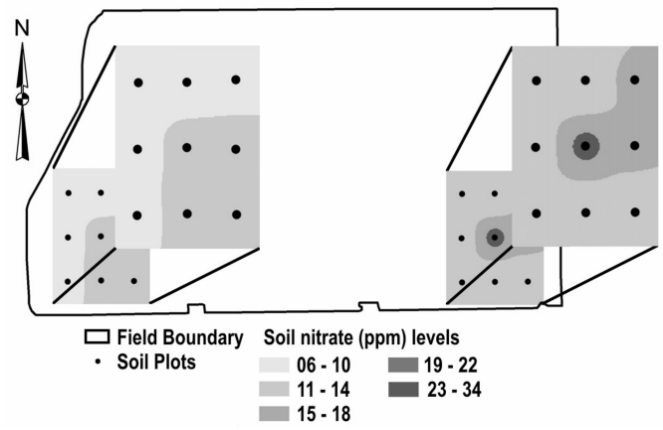

Fig. 4. Location of 18 sample plots with soil nitrate interpolation results using inverse distance weighting squared. The five soil nitrate levels were created using a k-means classifier.

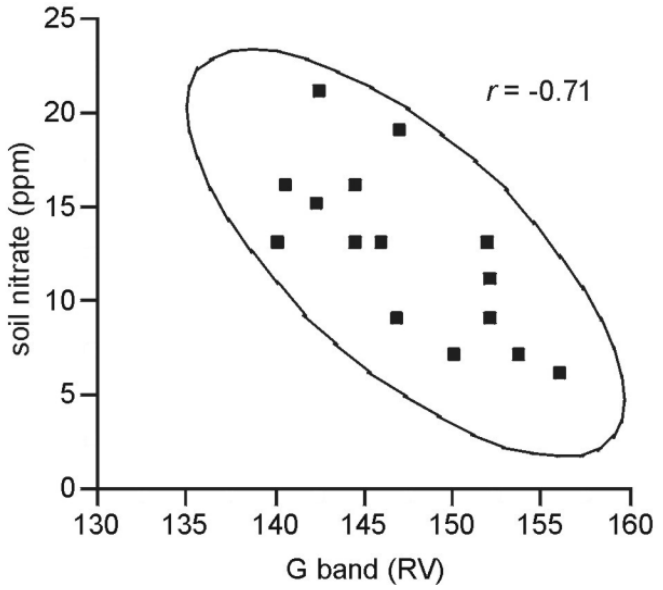

Fig. 5. Relationship between G image band (RV) and soil nitrate for sampled plots. Green reflectance increased as soil nitrate content decreased. Plants appeared visually darker in the green as soil N level increased.

tree species, more heterogeneous plant species below canopy, and more heterogeneous plant densities, or if spatial resolution is not high enough to avoid a mixture of soils, flowers, leaf shadows, and leaf senescence in a pixel. In comparison to soils, foliage coverage reduced visible reflectance because of chlorophyll absorption by the plant (Huete et al. 1984). Reflectance of flowers and senescent leaves was higher in both the R and G spectral regions. Foliage shadows and soil shadows both appeared dark in the R and G spectral regions. The unsupervised classification approach was able to separate green foliage within the canopy architecture from background noise.

Soil nitrate levels

Figure 4 shows the soil N interpolation results and the location of the 18 sample plots in the potato field. One condition that influenced soil N levels was spring flooding that caused water-logging in the soils over the study area. The water-logged soils facilitated denitrification and the leaching of soil N. In comparison to the southwest sampling area, the average soil N level was higher in the southeast sampling area. The area on the ground between interpolated soil N treatment levels was within 0.27 ha of one another.

The mean green RV of each plot sampled across all image acquisition dates was compared to the mean soil N samples taken on the 26th DAP (Fig. 5). Although there was up to a 35-day lag between soil N sampling and the final image acquisition date, the inverse linear relationship between foliage greenness and soil N (r = - 0.71) was significant. Soil N data were collected under an operational crop production setting. The applied soil N effects on foliage colour will not be immediate and a time lag is necessary to capture this effect. This inverse relationship between soil N and green foliage reflectance in the G spectral region is in agreement with previous studies (Blackmer et al. 1994; Boegh et al. 2002; Osborne et al. 2002;

Table 2. Correlation coefficient results for log Ψ_L and soil N with principal components for the training data set.

PC	Variability (%)	|r|	
		log Ψ_L	soil N (ppm)
1	4.70 x 10^{1}	0.33	0.37
2	3.11 x 10^{1}	0.29	0.42
3	2.13 x 10^{1}	0.04a	0.27
4	5.14 x 10^{-1}	0.44	0.07
5	1.03 x 10^{-1}	0.00	0.06
6	3.76 x 10^{-2}	0.22	0.27
7	5.64 x 10^{-3}	0.09b	0.09
8	1.77 x 10^{-3}	0.11	0.25
9	1.34 x 10^{-3}	0.21	0.19
10	2.94 x 10^{-4}	0.01	0.03
11	2.43 x 10^{-4}	0.12c	0.11
12	1.16 x 10^{-5}	0.09b	0.06
13	5.24 x 10^{-8}	0.07b	0.20
14	1.85 x 10^{-9}	0.04a	0.03
15	1.56 x 10^{-10}	0.12c	0.03
16	3.23 x 10^{-15}	0.12c	0.02
17	1.88 x 10^{-17}	0.12c	0.02

a PC 14 ~PC 3 (Ψ_L |r| = 0.04)
b PC 12, 13 ~ PC7 (Ψ_L |r| = 0.09 ± 0.02)
c PC 15 -, 17 ~PC 11 (Ψ_L |r| = 0.12)

Thomas and Oerther 1972). The significant inverse linear relationship between foliage greenness and soil N indicates that GRV's are an indicator of soil N levels.

Input neuron selection from principal components

Based on the assumption of normality required for the correlation matrix used in the PCA, all image variables with the exception of the H image parameter were identified as PCA candidates. The H image parameter was not normally distributed (W = 0.9279). The G image parameter, just inside the significance level for the F test, was kept for further analysis because of its relationship with soil N. The student's *t* test indicated that there was no significant difference between training and validation dataset means for any of the variables. PCA was then used to transform the normally distributed image variables into 17 principal components.

Input neuron selection for the ANN model used the training dataset and Pearson's correlation coefficient (*r*) to compare PCs with Ψ_L (Table 2). It was noted that in some cases, PCs with lower contributions towards total PCA variability exhibited higher correlations with measured Ψ_L than PCs with greater contributions towards total PCA variability. For example, PC 4, contained only 0.5% of the total PCA variability, but had the highest correlation with measured Ψ_L (r = |0. 44|). Other PCs with low contributions towards total PCA variability such as PC 6 and PC 9 contained only 0.038% and 0.0013% of the total PCA variability but indicated higher correlations with measured Ψ_L than other principal components. The second PC contained 31% of the total PCA variability and showed the third highest correlation with Ψ_L (r = |0.29|). The first PC showed the highest correlation with Ψ_L (r = |0.37|). Principal components 3, 5, 10, and 12 - 17 were omitted from the ANN model since, compared to other PCs with Ψ_L, they were within the same "family" as PCs retained as input neurons (Table 2). Correlations (*r*) of the principal components with Ψ_L were used to select eight of the PCs as input neurons in the ANN model to determine Ψ_L measurements.

Artificial neural network modeling

The artificial neural network (ANN) model was chosen as a method to relate the transformed image variables to the measured leaf water potential. The JMP IN (Version 5.1) software fits an ANN using standard nonlinear least-squares regression methods (SAS Institute 2002). The ANN model (8-2-1 ANN) consisted of 8 principal components using three layers: one input layer of neurons (one for each independent variable), one hidden layer of 2 neurons (the number which gave the optimal coefficient of determination) and one output layer of 1 neuron for leaf water potential (Ψ_L) as the dependent variable. Data for Ψ_L were log-transformed. The ANN modeling was used to address independence among the input neurons with measured Ψ_L.

To avoid the over-fitting problem inherent with ANN model design, the ANN model settings were empirically determined to establish the optimal coefficient of determination (R^2) and residual mean square error (RMSE) values. The problem of over-fitting data can result from using excessive hidden neurons. To attempt a global optimum, a number of tours or random starts can be applied to the ANN model. The number of iterations indicates the number of times a tour will run before reporting results of input neuron convergence. Thus to develop an ANN model with JMP IN, the ANN modeler should consider R^2, RMSE, the number of hidden neurons, the number of tours, and the over-fit penalty (SAS Institute 2002).

Results were evaluated to indicate that the ANN prediction model could successfully learn from the training data and successfully predict Ψ_L measures using a validation dataset. The ability of the ANN model to learn how to predict Ψ_L measures from the PC input neurons was achieved using the number of tours, R^2, and residual RMSE. With respect to the training dataset, 20 tours were used to obtain an R^2 of 0.82 and RMSE of 0.30 for the 8-2-1 ANN model to determine measured Ψ_L (Fig. 6). This indicated that the 8-2-1 ANN model was able to explain 82% of the total variation in predicted Ψ_L within ± 0.30.

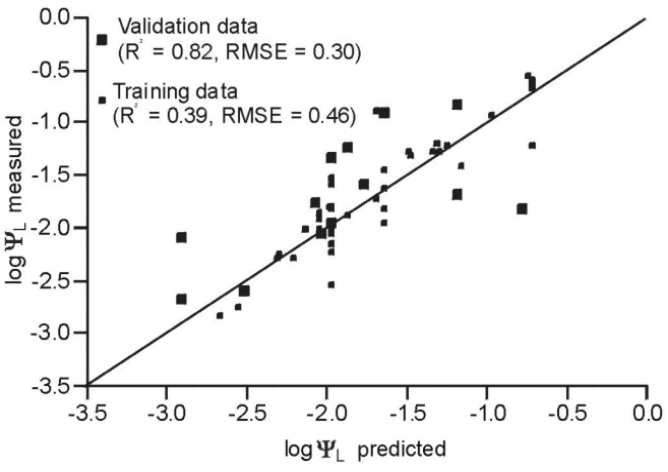

Fig. 6. Results for 8-2-1 ANN model for determining Ψ_L. The validation data points are shown in bold.

Table 3. Comparison of measured log Ψ_L and predicted log Ψ_L distributions for the validation dataset.

log Ψ_L	n	mean	SD	|CV|	Shaprio - Wilk		Bartlett's		Student's t test	
					W	p < W	F ratio	p > F	t ratio	p > |t|
measured	13	-1.75	0.57	32	0.97	0.83	0.14	0.71	-1.00	0.34
predicted	13	-1.90	0.63	33	0.95	0.60				

The R^2 and RMSE for the validation dataset (0.39 and 0.46, respectively) suggested that the ANN model was an unreliable predictor of Ψ_L at the plant level and was not unexpected. However, since irrigation occurs on a whole field basis, the ANN model need only predict a whole field Ψ_L average (Zakaluk and Sri Ranjan 2007). As a result, validation data were evaluated by comparing the mean and variance between the distributions for predicted Ψ_L and measured Ψ_L (Table 3). Given that the variance and mean between the distributions were not significantly different and that the CV's were similar, the predicted Ψ_L and measured Ψ_L were shown to be from common populations. Statistical evidence indicated that results can be used on well-watered potato plants, typically found in an irrigated field.

Since the *t* test indicated no significant difference between the means of measured and predicted Ψ_L (Table 3), the strength of the *t* test can be reviewed by calculating the smallest difference the *t* test was likely to detect (least significant value). Based on the variances and sample size used in the validation of the ANN model, the smallest detectable difference for the *t* test was 0.102 MPa and we can reasonably assume that both data sets were very similar.

Relative importance of input neurons

The responses of the eight principal components used as input neurons were assessed to determine their RI for the ANN model (Table 4). Figure 7 illustrates the RI of each ANN model input neuron. Figure 8 depicts a correlation curve for Ψ_L and soil N for each PC used in the ANN model ranked by relative importance. The fourth PC had the highest correlation with Ψ_L (r = |0.44|) and the lowest correlation with soil N (r = |0.07|). Consequently the fourth PC had the highest relative importance (RI = 11.15%). The second PC had the second highest correlation with Ψ_L (r = |0.29|). Although the second PC also had the strongest correlation with soil N (r = |0.42|), the separation between Ψ_L and soil N made it the second highest input neuron of relative importance (RI = 9.61%). Separation between correlations of Ψ_L and soil N with the eighth PC (r = |0.11| and r = |0.25|, respectively) made it the third highest input neuron of relative importance (RI = 6.98%). The remaining PCs (11, 1, 9, 7, and 6) showed lower differences between correlations with Ψ_L and soil N. In general, the PCs with more separation between Ψ_L and soil N correlations had more RI than PCs with less separation between Ψ_L and soil N correlations. Based on the RI analysis, it appears that when there is less separation between Ψ_L and soil N, the RI decreases, suggesting that soil N interacts with the determination of Ψ_L.

Table 4. Relative importance of input neuron connection weights with correlations against Ψ_L and soil N.

Input neuron	RI (%)	|r|	
		log Ψ_L	soil N (ppm)
PC 4	11.15	0.44	0.07
PC 2	9.61	0.29	0.42
PC 8	6.98	0.11	0.25
PC 11	6.66	0.12	0.11
PC 1	6.26	0.33	0.37
PC 9	5.62	0.21	0.19
PC 7	3.18	0.09	0.09
PC 6	0.55	0.22	0.27
PC 3	0.00	0.04	0.27
PC 5	0.00	0.00	0.06
PC 10	0.00	0.01	0.03

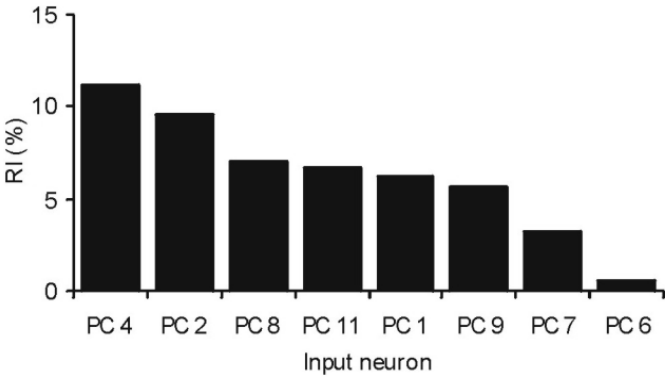

Fig. 7. Relative importance, in descending order, of each input neuron across the ANN model.

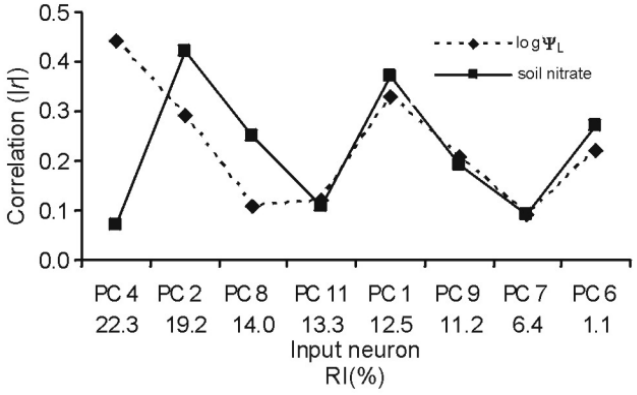

Fig. 8. Correlation curves for Ψ_L and soil N against relative importance (RI), in descending order, for each input neuron used in the ANN model. PC 4, PC 2, and PC 8 showed the most separation between Ψ_L and soil nitrate and the highest RL.

Table 5. Pearson's correlation coefficient (|r|) between image parameters and the field ANN model input neurons (ranked by relative importance).

Image parameter	Input neuron							
	PC 4	PC 2	PC 8	PC 11	PC 1	PC 9	PC 7	PC 6
X	0.15	0.40	0.00	4×10^{-5}	0.73	0.00	0.01	0.01
Y	0.13	0.73	0.00	6×10^{-4}	0.52	0.00	0.01	0.00
log G/B	0.03	0.41	0.00	3×10^{-5}	0.91	0.00	0.00	0.03
log B	0.00	0.73	0.00	4×10^{-4}	0.59	0.00	0.00	0.02
G	0.04	0.70	0.00	4×10^{-3}	0.25	0.01	0.01	0.02
GRS X	0.03	0.26	0.00	3×10^{-4}	0.02	0.00	0.00	0.01
log GBS	0.05	0.27	0.01	1×10^{-3}	0.80	0.00	0.01	0.02
log RBS	0.05	0.47	0.00	4×10^{-4}	0.88	0.00	0.01	0.02
log NDGBI	0.03	0.42	0.00	9×10^{-4}	0.91	0.01	0.00	0.02
I	0.01	0.87	0.01	4×10^{-3}	0.06	0.00	0.01	0.03
log S	0.01	0.32	0.01	4×10^{-4}	0.83	0.00	0.02	0.02
log R	0.05	0.92	0.01	2×10^{-4}	0.32	0.00	0.00	0.01
G/R X	0.12	0.73	0.00	1×10^{-3}	0.24	0.00	0.00	0.00
Z	0.01	0.28	0.00	5×10^{-4}	0.96	0.00	0.00	0.01
log R/B	0.04	0.10	0.00	3×10^{-4}	0.97	0.00	0.00	0.03
NDGRI X	0.14	0.73	0.00	1×10^{-3}	0.24	0.00	0.00	0.00
log NDRBI	0.03	0.10	0.00	6×10^{-4}	0.97	0.00	0.02	0.02

Image parameter loadings of input neurons

Pearson's correlation coefficient (r) was used to justify the eight PCs used as input neurons in the ANN model by comparing image parameter loadings of the PCs, comparing the PCs with Ψ_L, soil N, and radiometric calibration error (I) across images (Table 5). The highest loadings for the image parameters were found in PC 1, PC 2, and PC 4. Although no strong relationship can be identified between the image parameters and PC 4 ($r >$ |0.15|), the separation between soil N and Ψ_L indicated that PC 4 was a separator between the two measured biophysical factors (Fig. 8). A comparison of the difference in correlations between the PC 1 and PC 2 image parameter loadings suggested that red-blue and green-blue relationships were stronger in PC 1, while green-red relationships were stronger in PC 2. In addition, PC 2 contained the highest correlation with the green (G) image band (r = |0.70|), an indicator of soil N (r = |0.71|). The higher correlation for I in PC 2 in comparison to PC 1 (r = |0.87| versus r = |0.06|) indicated that despite the higher correlation of PC 1 with Ψ_L than PC 2 (Fig. 8), it can be concluded that soil N, as indicated by G, and radiometric calibration error as indicated by I, were the drivers for PC 2 that resulted in its higher relative importance in the ANN model.

Input neuron selection from the PCs required more than an examination of their contribution towards total variability and image parameter loading. For example, although PCs 6 – 9 and PC 11 lacked contributions towards total variability and lacked identifiable image parameter loadings, they were nevertheless required in the ANN model due to their relationship with Ψ_L and soil N (Fig. 8). For example, PC 8 contained low correlations with all input image parameters, and yet due to the separation it provided between Ψ_L and soil N (Fig. 8), it was the third most important input neuron in the ANN model. PCs that contained large amounts of the total PC variability with readily apparent image loadings was insufficient justification for their use. For example, PC 3 accounted for 29% of the total PC variability but had a low correlation with Ψ_L (r = |0.04|) and redundant correlation with PC 6 and soil N r = |0.27|). In addition, previous research indicated that the third PC, derived from RGB image bands, was related to soil clay content (Chen et al. 2004). Since soils, a biophysical parameter, were eliminated by image classification and PC 3 had a redundant correlation with PC 6, PC 3 was not required in the ANN model. The PCs with no identifiable image parameter loadings or relationships with Ψ_L or soil N are likely due to biophysical factors not measured in this study such as: leaf age, leaf structure, and soil nutrients. Further study into other biophysical parameters with the PCs is required to account for their use in the ANN model. The PC omissions as input neurons require analysis beyond image parameter loadings or contributions towards total variability.

Summary of findings

This research demonstrated the following:

1. The effects of shadow, soils, leaf senescence, and flowers could be isolated from green leaf foliage using an unsupervised classification approach.
2. An inverse linear relationship was found between soil N and leaf reflectance in the green image band.
3. The measured Ψ_L and predicted Ψ_L validation datasets were from common populations and therefore ANN modelling of Ψ_L using RGB images shows promise as a tool for determining an average Ψ_L across a potato field for irrigation scheduling.
4. Input neurons with more separation between Ψ_L and soil N were more important in the prediction of Ψ_L, suggesting that soil N interacts with Ψ_L prediction when using RGB images.
5. The ground-based digital camera was able to supply RGB images as an alternative to airborne-spaceborne imaging sensors.

These findings were similar to the results from an earlier greenhouse study (Zakaluk and Sri Ranjan 2007).

DISCUSSION

The results of this research may be explained in reference to visible light and stomatal opening via guard cell chloroplasts. While guard cell chloroplasts are responsive to the red region (Olsen et al. 2002), guard cell chloroplasts are primarily stimulated by the blue region with the size of the stomatal opening following the level of visible light incident upon the leaf surface (Zeiger et al. 2002). Kleman and Fagerlund (1987) found that the Z chromaticity coordinate, a transformation of the blue spectral region, could be used to separate irrigated and unirrigated barley (*Hordeum distichum* L.) under field conditions. Schlemmer et al. (2005) found that compared to the red spectral region, corn (*Zea mays* L.) leaves had a closer inverse linear relationship with relative water content (RWC) in the blue spectral region. Carter (1991) found that RWC was sensitive to the blue and red visible wavelengths centered at 480

and 680 nm for the leaves of six species. Given that the blue and red regions influence stomatal opening via guard cell chloroplasts and thus changes in Ψ_L due to water transpiration via the stomata, the prediction of Ψ_L using PCA of R and B combinations is justified.

The green image band was an important contributor of visible light reflectance to the determination of Ψ_L. This study was in agreement with previous studies (Schlemmer et al. 2005; Boegh et al. 2002; Osborne et al. 2002; Blackmer et al. 1994; Thomas and Oerther 1972) which showed that the green spectral region had a linear association with N. While high soil N was associated with dark green color, low soil N was associated with leaf yellowing. Incorporating the green image band into the PCA contributed to the establishment of relationships between principal components, soil N, and Ψ_L, enabling the ANN model to differentiate soil N from Ψ_L within the plant.

Monitoring chlorophyll absorption

While it might be argued that determining plant water stress in the visible region via plant chlorophyll could be influenced by other plant physiological factors (Carter 1991; Ceccato et al. 2001, 2002a, 2002b; Ripple 1986), strictly measuring plant water content inside the SWIR region limits the possibility of identifying plant stress beyond plant water deficits. For example, there is no benefit to applying additional nitrogen over a low nitrogen area if the crop is under water stress (Christensen et al. 2005; Ebertseder et al. 2005). Ideally, for optimal crop production, a remotely-sensed imaging model should also be developed to detect plant water stress and other plant physiological factors.

This study indicated that a physiological change due to soil N levels could be detected and isolated from the determination of Ψ_L using visible light and an ANN model design. While future research using the protocol in this study may result in agreement that visible leaf reflectance is not adequate for plant water stress detection, it may also be found that the only change, if any, may be in the ranking of the relative importance for the input neuron weights in the determination of plant water stress versus other plant physiological parameters. Moshou et al. (2003) used ANN modeling of five wavebands in the visible and NIR region to detect winter wheat (*Triticum sp* L.) stress under different soil N levels and yellow rust (*Puccinia striiformis* f. sp *tritici*) disease under field conditions. The use of ANN modeling of remotely sensed images to monitor plant stress shows promise for the detection of plant water stress and plant disease under different soil N levels. Based on findings from this study, further research is required to determine if other plant physiological factors and other soil atmosphere factors could be isolated from the determination of Ψ_L using RGB images, an ANN modeling approach, and relative importance analysis.

Sensor selection: Ground-based versus airborne-spaceborne image acquisition

The results of this study may be attributed to the short atmospheric transmission path (2.5 m), 0.91 mm spatial resolution data, and short timeline between image acquisition and in situ Ψ_L measurement which may not be transferable to lower spatial resolution images acquired by aircraft or satellite. Satellite based images are susceptible to atmospheric error due to the transmission path. In fact, wavebands on spaceborne imaging sensors are selected to avoid atmospheric transmission issues (Jensen 2005). While aircraft can design their imaging missions to avoid atmospheric haze and clouds with more flexibility than satellite imaging, satellite imaging relies on fixed revisit rates that can only resolve haze and cloud cover issues with the addition of more satellites. Images acquired with aircraft are also susceptible to hotspots caused by selecting the wrong combination of season and time of day for image acquisition (Avery and Berlin 1992). Hotspots in the airborne image create "whiteout" areas, which can make the image impossible to analyze.

According to Klotz et al. (2003), the use of a reference for reflectance values captured with a ground operated sensor eliminates the need for atmospheric correction models. To evaluate the radiometric calibration technique used in this study, the coefficient of variation (CV) for intensity (I) was determined. Intensity (I) is a measure of the mean for the distribution of reflectance across an image that is not associated with any color and is hence an indicator of reflectance that ignores the RGB "colors" used in this research. As a result, radiometrically calibrated multi-temporal RGB images should have similar intensities. The CV for intensity in this study indicated that the radiometric calibration error across all images did not exceed 4.99%.

Kostrzewski et al. (2002) reported that lower spatial resolutions smooth and reduce data variance, which supports the need to choose an appropriate spatial resolution fitting for the study objectives. The use of aircraft or satellite images for the determination of Ψ_L would be a source of error in the development of the ANN model because of the lower spatial resolution and the time lag between image acquisition and in situ Ψ_L measures. In this study, a digital camera mounted on a 2.5 m telescopic pole was used to eliminate the need for atmospheric correction through the use of standardized reflectance reference and to optimize revisit rates to synchronize with in situ measures of Ψ_L. If future research using airborne or spaceborne imaging sensors to determine Ψ_L is to follow the protocol employed in this study, then the lower spatial resolution, limited revisit rates, and atmospheric correction will need to be considered.

Experimental error associated with leaf water potential and soil N

Results for the |CV| were 32% and 33% for both the measured Ψ_L and predicted Ψ_L datasets, respectively (Table 3). According to Gomez and Gomez (1984), the CV is an indicator of experimental error and the acceptability of the CV depends on the type of experiment. The CV for Ψ_L field data in research conducted by Blad and Walter-Shea (1994) was between 62% and 85% for five grassland species collected over the Konza Prairie in Kansas. In another field study of Ψ_L measurements on forest species (Almeida 2000), results indicated that experimental error for predawn Ψ_L measurements (CV = 47%) versus midday Ψ_L measurements (CV = 40%) was greater. This appears reasonable since during the midday period, sunlight is at a maximum, and stomatal resistance would be greater. In addition to the time of day for taking Ψ_L measurements, Naor et al. (2006) reported that variability in midday Ψ_L measurements can be avoided by considering subfield variation caused by irrigation or soil hydraulic properties, sample storage, and human error of Ψ_L measurement.

In this study, Ψ_L measurements were taken from soil N plots between the morning and late afternoon and thus contributed to the experimental error. However, by ignoring soil N and randomly selecting plots throughout the trial period, Ψ_L measurements across plots were not biased by soil N. For example, if all low soil N plots were measured for Ψ_L during the morning, while all high soil N plots were measured for Ψ_L at midday, there may have been some bias towards higher soil N plots obtaining lower experimental error due to Ψ_L measurement. To minimize experimental error, Ψ_L measurements ideally should only be collected during the midday period. Based on Almeida (2000) and Blad and Walter-Shea (1994), the CV of Ψ_L measurements for this study were nevertheless within acceptable limits for this type of research.

CONCLUSION

This study examined RGB images, vegetation indices, and image transformations derived from a ground based five megapixel RGB single CCD chip digital camera to determine if Ψ_L could be predicted for field potatoes. Existing soil N levels were predetermined at each plot to account for soil N interaction with measured Ψ_L.

Although the number of field samples was limited, a number of conclusions was reached in this study. Using 0.91 mm spatial resolution images and under homogeneous plant conditions, the G and R image bands could be used to separate green foliage from shadow, soils, leaf senescence, and flowers. A significant inverse linear relationship between green foliage as measured by the green image band and soil N was found ($\alpha \leq 0.05$). The ground based five megapixel RGB digital camera provided comparable distributions, means, and variances between measured Ψ_L and predicted Ψ_L using ANN modeling. PCA performed on the RGB images and six image transformations and nine vegetation indices found principal components with both similar and different linear relationships with either measured Ψ_L or measured soil N. The principal components with the greatest separation between measured Ψ_L and measured soil N were the most important input neurons for predicting Ψ_L using ANN modeling of RGB images. The digital camera was found to be a viable option to airborne and spaceborne images acquisition methods.

Study findings may be attributable to the 0.91 mm spatial resolution images, the number of measurements used in the study, and/or the physiological relationships between the visible light reactions and water stress for potatoes. It remains unclear how well the ANN modeling protocol will succeed across other crops consisting of different canopy structures. Given the exploratory nature of this study, further research is required to validate the protocol and stability of input neuron RI before implementation into a potato plant water stress monitoring program.

ACKNOWLEDGEMENTS

This research was financially supported in part by Red River College through a grant funded by Western Economic Diversification Canada. The authors thank Frank Elias with Kroeker Farms Limited for his invaluable assistance in making the potato field research possible.

REFERENCES

Almeida, D. 2000. LBA water potential data. http://ecophys.biology.utah.edu/public/LBA/Water_potential_data/ (2007/02/02).

Asrar, G., M. Fuchs, E.T. Kanemasu and J.L. Hatfield. 1984. Estimating absorbed photosynthetic radiation and leaf area index from spectral reflectance in wheat. *Agronomy Journal* 76: 300-306.

Avery, T.E. and G.L. Berlin. 1992. *Fundamentals of remote sensing and airphoto interpretation,* 5th edition. Upper Saddle River, NJ: Prentice Hall.

Bastiaanssen, W.G.M. and M.G. Bos. 1999. Irrigation performance indicators based on remotely sensed data: A review of literature. *Irrigation and Drainage Systems* 13: 291-311.

Blackmer, T.M., J.S. Schepers and G.E. Meyer. 1994. Remote sensing to detect nitrogen deficiency in corn. In *Proceedings of Site-Specific Management for Agricultural Systems*, 505-512. Minneapolis, MN: ASA/CSSA/SSSA.

Blad, B.L. and E.A. Walter-Shea. 1994. Total Leaf Tissue Water Potential (FIFE) Data set. http://www.daac.ornl.gov (2007/02/05).

Boegh, E., H. Soegaard, N. Broge, C.B. Hasager, N.O. Jensen, K. Schelde and A. Thomsen. 2002. Airborne multispectral data for quantifying leaf area index, nitrogen concentration, and photosynthetic efficiency in agriculture. *Remote Sensing of Environment* 81: 179-193.

Bowman, W.D. 1989. The relationship between leaf water status, gas exchange, and spectral reflectance in cotton leaves. *Remote Sensing of Environment* 30: 249-255.

Carter, G. 1991. Primary and secondary effects of water content on the spectral reflectance of leaves. *America Journal of Botany* 78: 916-924.

Ceccato, P., S. Flasse, S. Tarantola, S. Jacquemound and J.M. Gregoire. 2001. Detecting vegetation leaf water content using reflectance in the optical domain. *Remote Sensing of Environment* 77: 22-33.

Ceccato, P., N. Gobron, S. Flasse, B. Pinty and S. Tarantola. 2002a. Designing a spectral index to estimate vegetation water content from remote sensing data Part 1. Theoretical Approach. *Remote Sensing of Environment* 82: 188-197.

Ceccato, P., S. Flasse and J.M. Gregoire. 2002b. Designing a spectral index to estimate vegetation water content from remote sensing data Part 2. Validation and applications. *Remote Sensing of Environment* 82: 198-207.

Charles-Edwards, D.A., D. Doley and G.M. Rimmington. 1986. *Modelling Plant Growth and Development.* Orlando, FL: Academic Press.

Chen, F., D.E. Kissel, L.T. West and W. Adkins. 2004. Field scale mapping of surface clay concentration. *Precision Agriculture* 5: 7-26.

Christensen, L.K., D. Rodriguez, R. Belford, V. Sadras, R. Rampart and P. Fisher. 2005. Temporal predictions of nitrogen status in wheat under the influence of water deficiency using spectral and thermal information. In *Proceedings of the Fifth European Conference on Precision*

Agriculture, 209-215. Uppsala, Sweden: Swedish Institute of Agricultural and Environmental Engineering/Swedish University of Agricultural Sciences.

Costa, L.D., G.D. Vedove, G. Gianquinto, R. Giovanardi and A. Peressotti. 1997. Yield, water use efficiency and nitrogen uptake in potato: Influence of drought stress. *Potato Research* 40: 19-34.

del Moral, R. 1975. Vegetation clustering by means of ISODATA: Revision by multiple discriminate analysis. *Plant Ecology* 29: 179-190.

Eastman, J.R. and M. Fulk. 1993. Long sequence time series evaluation using standardized principal components. *Photogrammetric Engineering & Remote Sensing* 59: 991-996.

Ebertseder, Th., U. Schmidhalter, R. Gutser, U. Hege and S. Jungert. 2005. Evaluation of mapping and on-line nitrogen fertilizer application strategies in multi-year multi-location static field trials for increasing nitrogen use efficiency of cereals. In *Proceedings of the Fifth European Conference on Precision Agriculture,* 327-335. Uppsala, Sweden: Swedish Institute of Agricultural and Environmental Engineering/Swedish University of Agricultural Sciences.

Gamon, J.A. and J.S. Surfas. 1999. Assessing leaf pigment content and activity with a reflectometer. *New Phytologist* 143: 105-117.

Gevrey, M., I. Dimopoulos and S. Lek. 2003. Review and comparison of methods to study the contribution of variables in artificial neural network models. *Ecological Modelling* 160: 249-264.

Gillespie, A.R., A.B. Kahle and R.E. Walker. 1987. Color enhancement of highly correlated images. II. Channel ratio and "chromaticity" transformation techniques. *Remote Sensing of Environment* 22: 343-365.

Gitelson, A., Y.J. Kaufman, R. Stark and D. Rundquist. 2002. Novel algorithms for remote estimation of vegetation fraction. *Remote Sensing of the Environment* 80: 76-87.

Gomez, K.A. and A.A. Gomez. 1984. *Statistical Procedures for Agricultural Research*. New York, NY: John Wiley & Sons, Inc.

Gonzalez, R.C. and R.E. Woods. 2002 *Digital Image Processing,* 2nd edition. Upper Saddle River, NJ: Prentice Hall.

Gunel, E. and T. Karadogan. 1998. Effect of irrigation applied at different growth stages and length of irrigation period on quality characters of potato tubers. *Potato Research* 41: 9-19.

Haboudane, D., J.R. Miller, N. Tremblay, P.J. Zarco-Tejada and L. Dextraze. 2002. Integrated narrow-band vegetation indices for prediction of chlorophyll content for application to precision agriculture. *Remote Sensing of Environment* 81: 416-426.

Huete, A.R., D.F. Post and R.D. Jackson. 1984. Soil spectral effects on 4-space vegetation discrimination. *Remote Sensing of Environment* 15: 155-165.

Ingebritsen, S.E. and R.J.P. Lyon. 1985. Principal components of multitemporal image pairs. *International Journal of Remote Sensing* 6: 687-696.

Jackson, T.J., D. Chen, M. Cosh, F. Li, M. Anderson, C. Walthall, P. Doriaswamy and E.R. Hunt. 2004. Vegetation water content mapping using Landsat data derived normalized difference water index for corn and soybeans. *Remote Sensing of Environment* 92: 475-482.

Jensen, J.R. 2005. *Introductory Digital Image Processing, a Remote Sensing Perspective,* 3rd edition. Upper Saddle River, NJ: Prentice Hall.

Kanemasu, E.T. 1974. Seasonal canopy reflectance patterns of wheat, sorghum, and soybean. *Remote Sensing of Environment* 3: 43-47.

Karimi, Y., S.O. Prasher, H. McNairn, R.B. Bonnell, P. Dutilleul and P.K. Goel. 2005. Discriminant analysis of hyperspectral data for assessing water and nitrogen stresses in corn. *Transactions of the ASAE* 48: 805-813.

Kleman, J.K. and E. Fagerlund. 1987. Influence of different nitrogen and irrigation treatments on the spectral reflectance of barley. *Remote Sensing of Environment* 21: 1-14.

Klotz, P., H. Bach and W. Mauser. 2003. GVIS ground operated visible/near infrared imaging spectrometer. In *Proceedings of the Fourth European Conference on Precision Agriculture*, 315-323. Berlin, Germany: Centre for Agricultural Landscape and Land Use Research/ Institute of Agricultural Engineering Bornim.

Kostrzewski, M., P. Waller, P. Guertin, J. Haberland, P. Colaizzi, E. Barnes, T. Thompson, T. Clarke, E. Riley and C. Choi. 2002. Ground-based remote sensing of water and nitrogen stress. *Transactions of the ASAE* 46(1): 29-38.

McCoy, R.M. 2005. *Field Methods in Remote Sensing*. New York, NY: The Guilford Press.

McMurtrey, J.E., E.W. Chappelle, M.S. Kim, J.J. Meisinger and L.A. Corp. 1994. Distinguishing nitrogen fertilizer levels in field corn (Zea mays L.) with actively induced fluorescence and passive reflectance measurements. *Remote Sensing of Environment* 47: 36-44.

Moshou, D., C. Bravo, S. Wahlen, J. West and A. McCartney. 2003. Simultaneous identification of plant stresses and diseases in arable crops based on a proximal sensing system and self organizing neural networks. In *Proceedings of the Fourth European Conference on Precision Agriculture,* 425-431. Berlin, Germany: Centre for Agricultural Landscape and Land Use Research/ Institute of Agricultural Engineering Bornim.

Naor, A., Y. Gal and M. Peres. 2006. The inherent variability of water stress indicators in apple, nectarine, and pear orchards, and the validity of a leaf-selection procedure for water potential measurements. *Irrigation Science* 24: 129-135.

Olsen, R.L., B.P. Pratt, P. Gump, A. Kemper and G. Tallman. 2002. Red light activates a chloroplast-dependent ion uptake mechanism for stomatal opening under reduced CO_2 concentrations in Vicia spp. *New Phytologist* 153: 497-508.

Osborne, S.L., J.S. Schepers, D.D. Francis and M.R. Schlemmer. 2002. Use of spectral radiance to estimate in-season biomass and grain yield in nitrogen- and water stressed corn. *Crop Science* 42: 165-171.

Penuelas, J., J.A. Gamon, A.L. Fredeen, J. Merino and C.B. Field. 1994. Reflectance indices associated with physiological changes in nitrogen- and water-limited sunflower leaves. *Remote Sensing of Environment* 48: 135-146.

Ripple, W.J. 1986. Spectral reflectance relationships to leaf water stress. *Photogrammetric Engineering and Remote Sensing* 52: 1669-1675.

Rzempoluck, E.J. 1998. *Neural Network Data Analysis Using Simulnet*™. New York, NY: Springer-Verlag.

SAS Institute. 2002. *Jmp Version 5 Statistics and Graphics Guide*. Cary, NC: Statistical Analysis System, Inc.

Schlemmer, M.R., D.D. Francis, J.F. Shanahan and J.S. Schepers. 2005. Remotley measuring chlorophyll content in corn leaves with differing nitrogen levels and relative water content. *Agronomy Journal* 97: 106-112.

Scholander, P.F., H.T. Hammel, E.D. Bradstreet and E.A. Hemminsen. 1965. Sap pressure in vascular plants. *Science* 148: 339-346.

Sony Corporation. 2004. ICX452AQF data sheet. http://www.eureca.de/pdf/optoelectronic/sony/ICX452AQF.PDF (2007/01/28).

Thomas, J.R. and G.F. Oerther. 1972. Estimating nitrogen content of sweet pepper leaves by reflectance measurements. *Agronomy Journal* 64: 11-13.

Tremblay, N., H. Scharpf, U. Weier, H. Laurence and J. Owen. 2001. Nitrogen Management in Field Vegetables - A guide to efficient fertilization. http://res2.agr.ca/stjean/publication/bulletin/nitrogen9-azote9_e.htm (2007/01/20).

Ustin, S.L. 2004. *Manual of Remote Sensing, Volume 4, Remote Sensing for Natural Resource Management and Environmental Monitoring,* 3rd edition. Hoboken, NJ: John Wiley & Sons, Inc.

Waring, R.H. and B.D. Cleary. 1967. Plant moisture stress, evaluation by pressure bomb. *Science* 155: 1248-1254.

Wheeler, R.M. 2006. Potato and human exploration of space: Some observations from NASA-sponsored controlled environmental studies. *Potato Research* 49: 67-90.

White, A.M., G.P. Asner, R.R. Nemani, J.L Privette and S.W. Running. 2000. Measuring fractional cover and leaf area index in arid ecosystems: Digital camera, radiation transmittance, and laser altimetry methods. *Remote Sensing of Environment* 74: 45-57.

Woebbecke, D.M., G.E. Meyer, K. Von Bargen and D.A. Mortensen. 1995. Color indices for weed identification under various soil residue and lighting conditions. *Transactions of the ASAE* 38: 259-269.

Zakaluk, R. and R. Sri Ranjan. 2007. Artificial neural network modelling of leaf water potential for potatoes using RGB digital images–A greenhouse study. *Potato Research* 49: 255-272.

Zeiger, E., L.D. Talbott, S. Frechilla, A. Srivastava and J. Zhu. 2002. The guard cell chloroplast: A perspective for the twenty-first century. *New Phytologist* 153: 415-424.

Zhurmar, A.Y. and E.A. Yanovskaya. 1992. Use of spectral information to estimate the mineral content of agricultural crops. *Soviet Journal of Remote Sensing* 10: 130-139.

LIST of SYMBOLS

AGL	above ground level (m)
ANN	artificial neural network
B	blue image band (8 bit)
CCD	charged couple device
CV	coefficient of variation (%)
DAP	days after planting
FC	field capacity or upper soil water limit allowable for plant growth
G	green image band (8 bit)
GBS	green blue slope (8 bit RV/nm)
GB	green blue simple ratio (dimensionless)
GPS	global positioning satellite
GR	green red simple ratio (dimensionless)
GRS	green red slope (8 bit RV/nm)
H	hue transformation (8 bit)
I	intensity transformation (8 bit)
N	nitrate (ppm)
NDGBI	normalized difference green blue index (dimensionless)
NDGRI	normalized difference green red index (dimensionless)
NDRBI	normalized difference red blue index (dimensionless)
p	probability level
PC	principal component
PCA	principal component analysis
PWL	peak wavelength (nm)
R	red image band (8 bit)
r	correlation coefficient
R^2	coefficient of determination
RB	red blue simple ratio (dimensionless)
RBS	red blue slope (8 bit RV/nm)
RMSE	residual mean square error
RGB	red green blue regions of the electromagnetic spectrum
RWC	relative water content a soil (%)
RI	relative importance of input neuron (%)
RV	reflectance value response from an image (8 bit)
TDR	time domain reflectometry
S	saturation transformation (8 bit)
SR	simple ratio vegetation index
W	Shapiro-Wilk test for normality
X	chromaticity color coordinate transformation
Y	chromaticity color coordinate transformation
Z	chromaticity color coordinate transformation
α	significance level
Ψ_L	leaf water potential (MPa)
θ_V	volumetric water content (%)